Supporting Information

Insights into the Redox Behavior of $Pr_{0.5}Ba_{0.5}MnO_{3-\delta}$ Derived Perovskites for CO_2 Valorization Technologies

Andrea Felli[a], *Silvia Mauri*[b,c], *Marcello Marelli*[d], *Piero Torelli*[b], *Alessandro Trovarelli*[a], *and Marta Boaro*[a,*].

[a]Dipartimento Politecnico, University of Udine, Via del Cotonificio 108, 33100, Udine, Italy.

[b]CNR - Istituto Officina dei Materiali, TASC, 34149, Trieste, Italy.

[c]Department of Physics, University of Trieste, Via Valerio 2, 34127 Trieste, Italy.

[d]CNR-SCITEC, Istituto di Scienze e Tecnologie Chimiche "Giulio Natta", Via G Fantoli 16-15, 20138 Milan, Italy.

[*]marta.boaro@uniud.it

Chemical-physical characterization

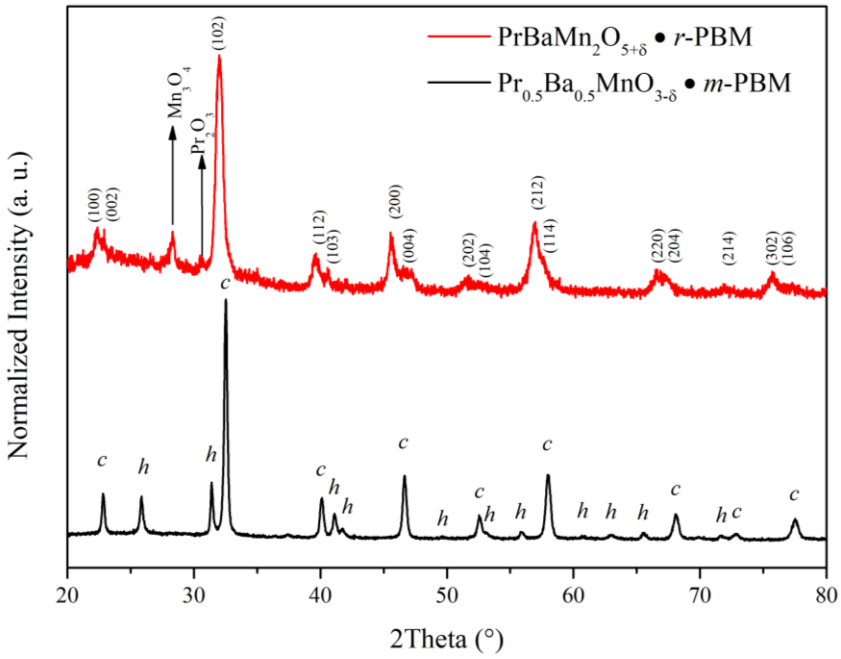

Figure S1. XRD spectra of *m*-PBM ($Pr_{0.5}Ba_{0.5}MnO_{3-\delta}$, black), and *r*-PBM ($PrBaMn_2O_{5+\delta}$, red) cooled in reducing atmosphere. The segregation of Mn_3O_4 and Pr_2O_3 is evidenced. The segregation was eliminated by the oxidation of *r*-PBM phase at high temperature and the formation of $PrBaMn_2O_{6-\delta}$. (*c*): cubic phase. (*h*): hexagonal phase.

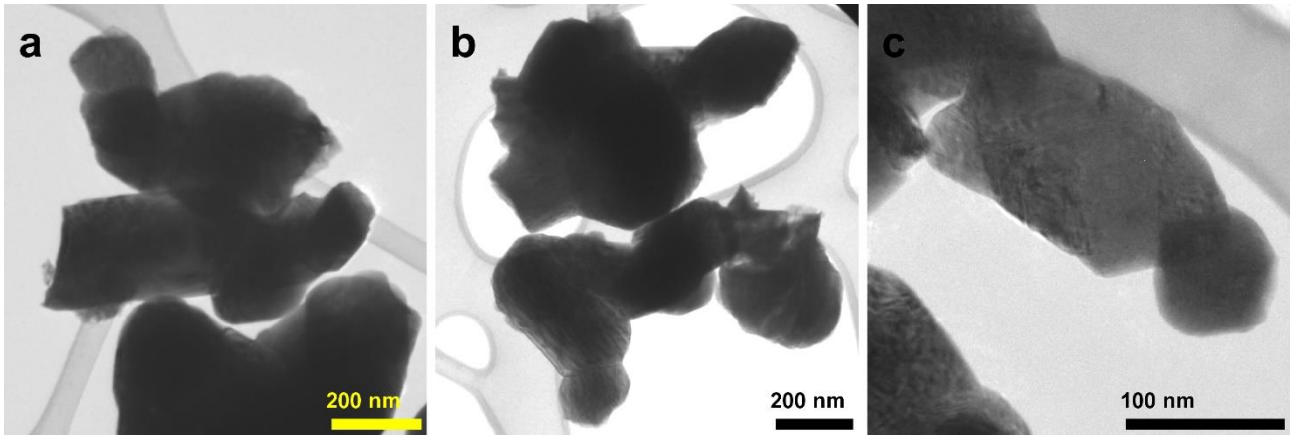

Figure S2. Representative TEM micrographs of a) *m*-PBM ($Pr_{0.5}Ba_{0.5}MnO_{3-\delta}$), b) *o*-PBM ($PrBaMn_2O_{6-\delta}$) and c) *r*-PBM ($PrBaMn_2O_{5+\delta}$).

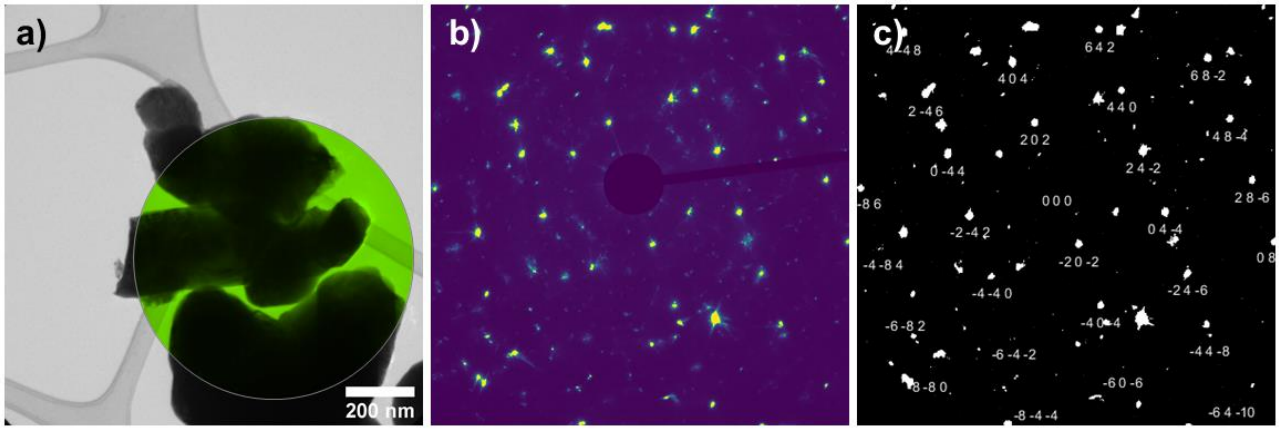

Figure S3. *m*-PBM electron diffraction analysis of selected sample area (highlighted in green in first TEM micrograph) - b), related electron diffraction pattern in false colors and c) pattern indexing of main single-crystal spots assigned to $Pr_{0.5}Ba_{0.5}MnO_{3-\delta}$ – zone axis -1 1 1.

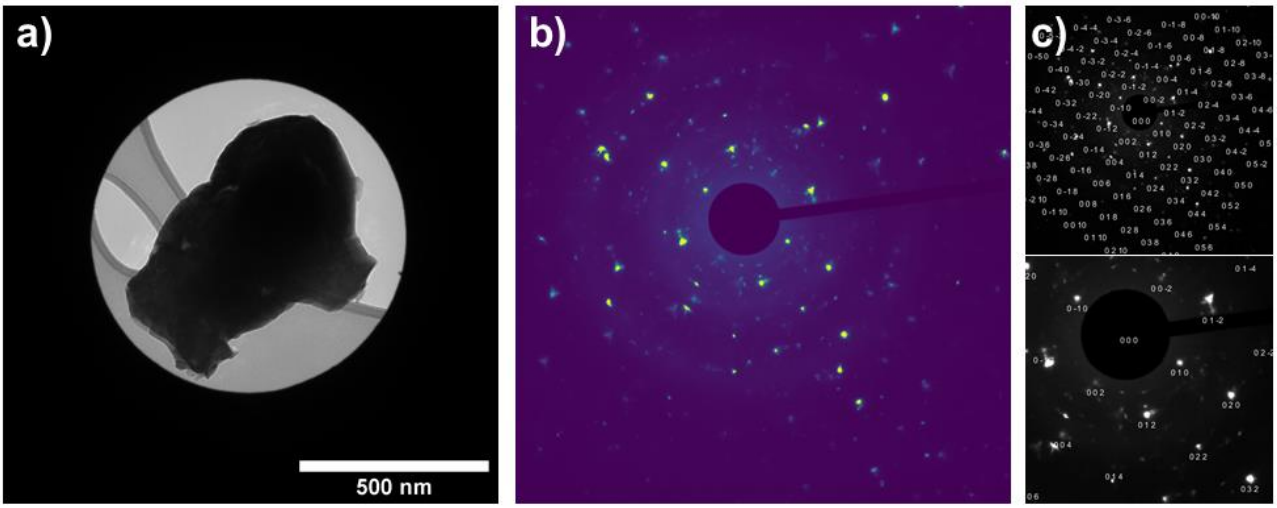

Figure S4. *o*-PBM electron diffraction analysis of selected sample area - b), related electron diffraction pattern in false colors and c) pattern indexing of main single-crystal spots assigned to $PrBaMn_2O_{6-\delta}$ – zone axis 1 0 0.

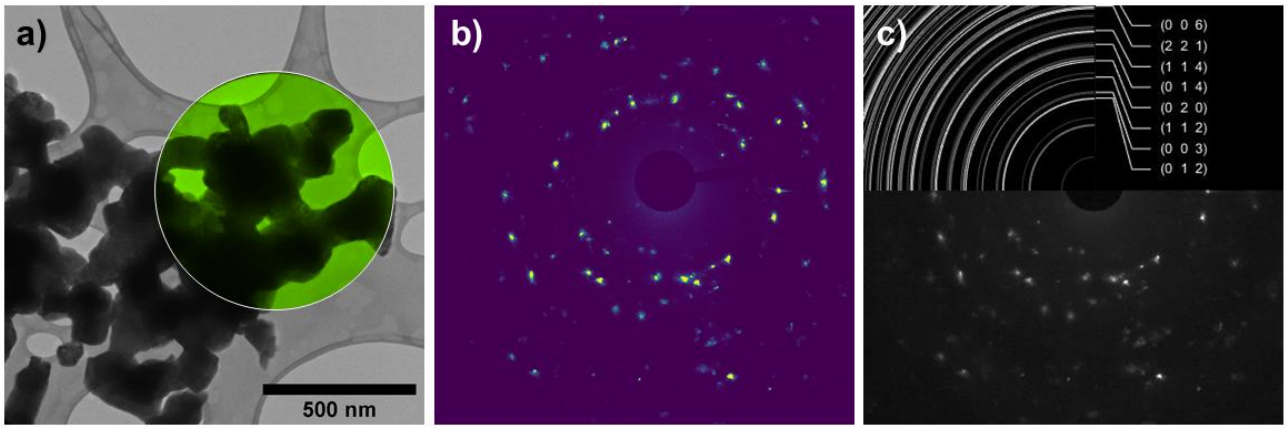

Figure S5. *r*-PBM electron diffraction analysis of selected sample area (highlighted in green in first TEM micrograph) - b), related electron diffraction pattern in false colors and c) pattern indexing of poly-crystalline spots assigned to $PrBaMn_2O_{5+\delta}$. The superimposed rings are part of the simulated pattern.

N. B.: The SAED analysis in Figure S3, S4 and S5 was performed by software CrysTBox diffractGUI 2.21 by Miloslav Klinger[1]

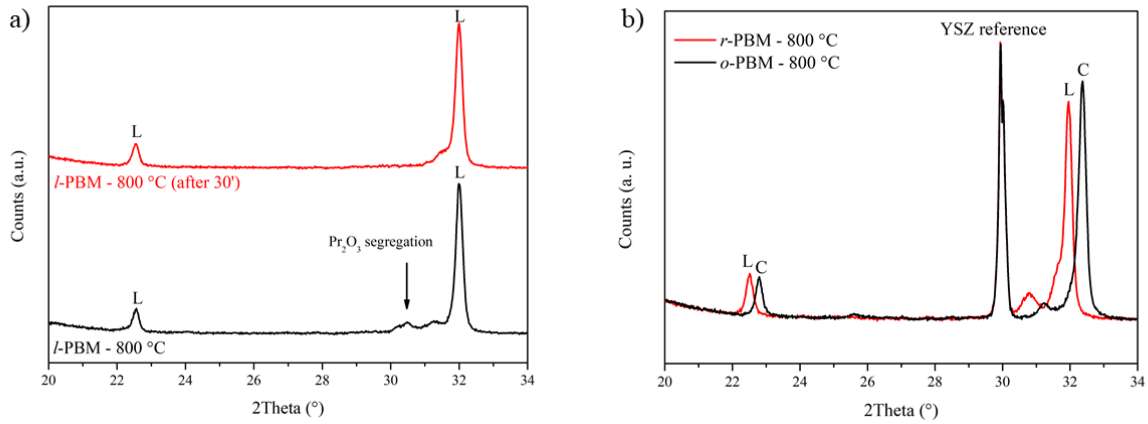

Figure S6. *In situ* XRD patterns between 20° to 34° of a) *r*-PBM before (black) and after a dwell of one hour at 800 °C (red); b) *r*-PBM (black) and its oxidation at 750 °C to form *o*-PBM (red); a YSZ (Yttria Stabilized Zirconia) pellet was used as internal reference, to discriminate between contributions due to temperature changes and expansion of lattice.

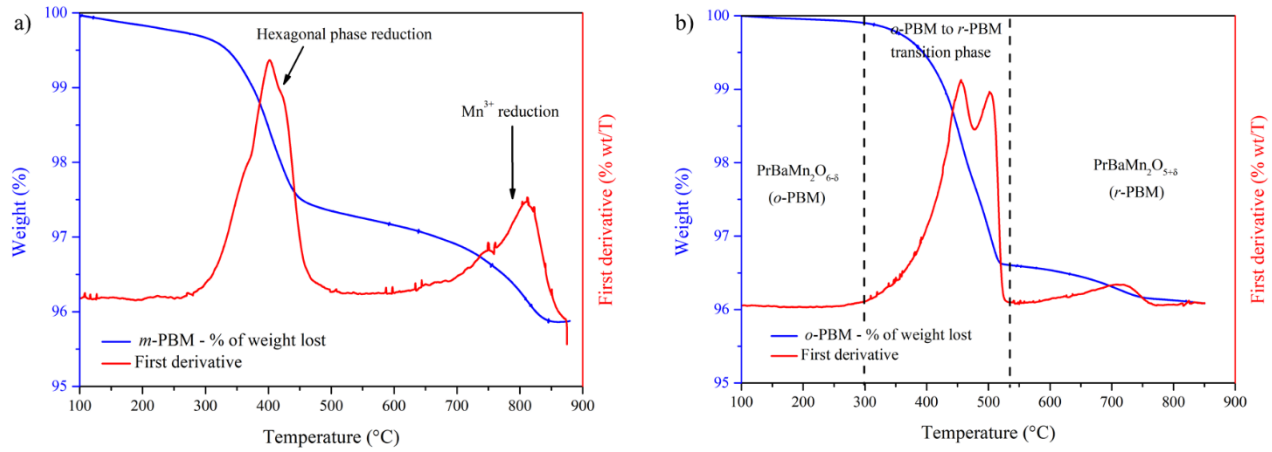

Figure S7. Weight variation (blue) and its first derivative (red) a) for the first cycle and b) for the second cycle during the TGA experiment in air.

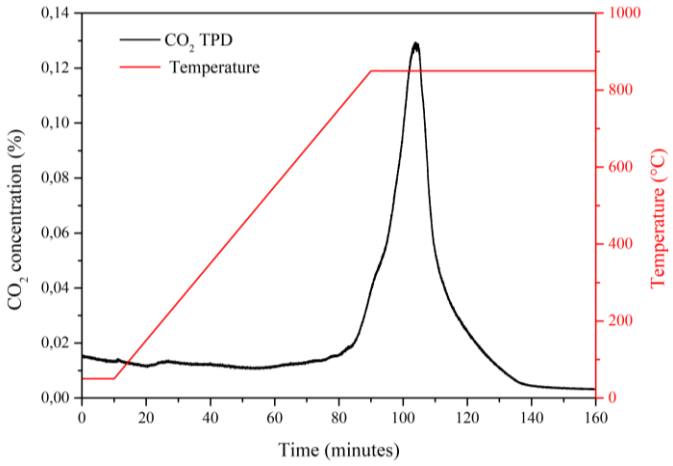

Figure S8. CO_2 TPD in N_2 (100%). The release of CO_2 was detected using a mass spectrometer, from 50 °C to 850 °C, 10 °C·min^{-1}. The sample was maintained for ~ 1 hour at 850 °C.

Electrochemical characterization

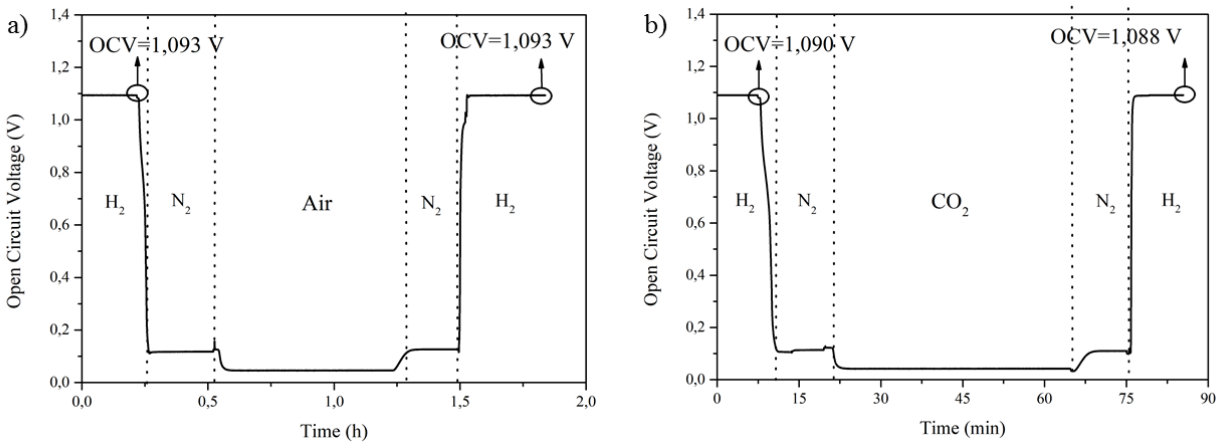

Figure S9. OCV variation for a *r*-PBM//YSZ//LSM button cell during a redox cycle at 850°C: a) H_2/air cycle, b) H_2/CO_2 cycle. Flow: 20% H_2 in N_2 (100 mL·min^{-1}), air and CO_2 (100 mL·min^{-1}).

Figure S9 shows the open circuit voltage (OCV) signal during a redox cycle at 850 °C, using both air (Figure S9 a) and pure CO_2 (Figure S9 b) as oxidizing gases; the initial value of 1.093 V near the Nernst potential reveals good reversibility of the *r*-PBM electrode for the HER reaction and provides indication of the initial integrity of the cell and its seal.

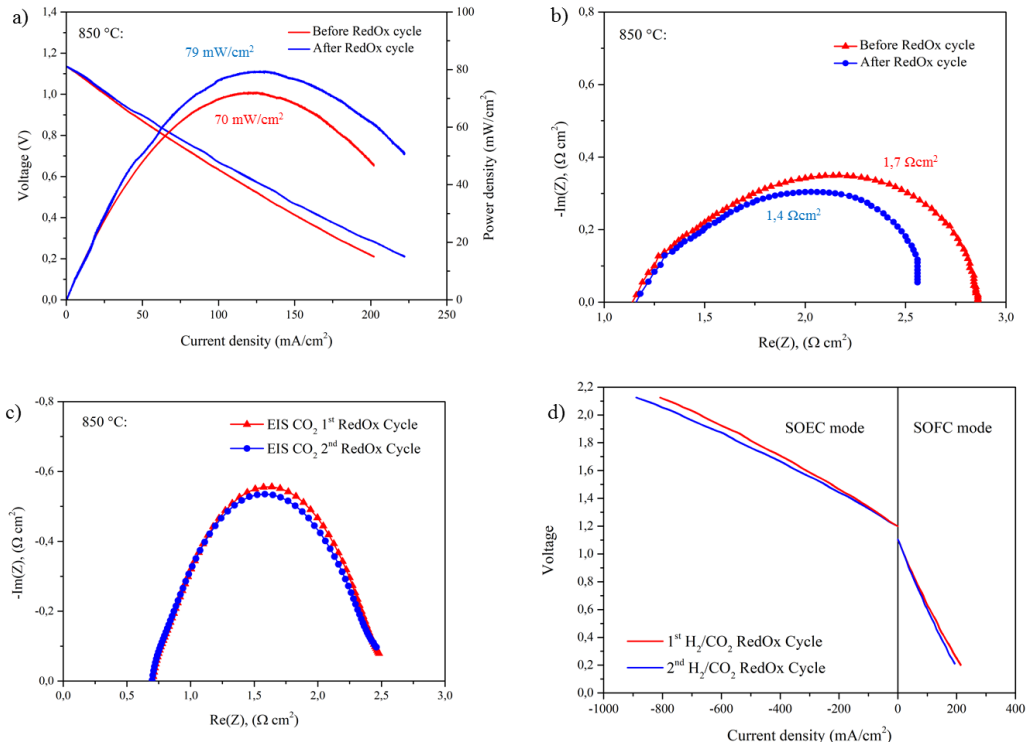

Figure S10. *r*-PBM//YSZ//LSM button cells performances at 850°C in pure H_2: a) VI and PI curves before (red) and after (blue) an oxidation step in air; b) Electrochemical Impedance Spectroscopy (EIS) characterization as Nyquist plots before (red) and after (blue) an air oxidation step; c) Nyquist plots under SOEC operation mode in pure CO_2 at 850 °C, after a first (red) and a second (blue) SOFC/SOEC cycle d) linear polarization curve in SOFC (right) and SOEC (left) mode after a first (red) and second (blue) H_2- SOFC/CO_2-SOEC cycle.

Figure S10 compares VI and PI curves (a) and EIS Nyquist plots (b) of a r-PBM/YSZ/LSM cell in 100% H_2 at 850°C before (red) and after (blue) a redox cycle. A slight increase in cell performance (from 70 $mW \cdot cm^{-2}$ to 79 $mW \cdot cm^{-2}$) with a corresponding decrease in the total polarization value (1.7 $\Omega \cdot cm^2$ and 1.4 $\Omega \cdot cm^2$) was observed after the redox cycle, probably due to a favorable reorganization of the electrode surface. No changes in the ohmic resistance value (R_Ω) were observed indicating that the exposure to air did not damage the electrolyte/electrode interface and the collectors.

The performance of the cell is low compared to literature references[2,3], but it needs to note that no attempts were made to optimize the electrodes morphology and the quality of the interfaces for this study. Moreover, the thickness of the electrolyte concurred to introduce a large ohmic resistance. Figure S10 c reports the Nyquist plots of a *r*-PBM//YSZ//LSM button cell tested in SOEC mode in

pure CO_2 at 850°C. No visible variation in terms of total polarization occurred between the two SOFC/SOEC cycles; a ~1.78 $\Omega \cdot cm^2$ total polarization was estimated from the two impedance spectra.

Figure S10 d shows the activity of *r*-PBM//YSZ//LSM cell tested in different operation mode after two successive SOEC/SOFC cycles. In SOFC mode the maximum current density slightly decreased (from 110.1 $mA \cdot cm^{-2}$ to 108.4 $mA \cdot cm^{-2}$) from the first cycle (red curve) to the second cycle (blue curve)). This was probably due to the formation of surface carbonates during the electrode exposure to CO_2. Conversely in SOEC mode a slight improvement in performance was observed (227.2 $mA \cdot cm^{-2}$ vs. 218.7 $mA \cdot cm^{-2}$), probably associated to a more appropriate distribution of defects after the redox cycles. All over only small and almost negligible changes in the performances were observed. Therefore, it is inferred that phase transition which occurs during the switch of atmosphere and mode does not involve significant deterioration of the PBM based electrode.

References

(1) Klinger, M.; *J. Appl. Crystal.*, **2017**, *50*, 1226 (2017).

(2) Sengodan, S.; Choi, S.; Jun, A.; Shin, T. H.; Ju, Y. W.; Jeong, H. Y.; Shin, J.; Irvine, J. T. S.; Kim, G. Layered Oxygen-Deficient Double Perovskite as an Efficient and Stable Anode for Direct Hydrocarbon Solid Oxide Fuel Cells. *Nat. Mater.* **2015**, *14* (2), 205–209. https://doi.org/10.1038/nmat4166.

(3) Shin, T. H.; Myung, J.; Verbraeken, M.; Kim, G.; Irvine, J. T. S. Oxygen Deficient Layered Double Perovskite as an Active Cathode for CO_2 Electrolysis Using a Solid Oxide Conductor. *Faraday Discuss.* **2015**, *182* (0), 227–239. https://doi.org/10.1039/c5fd00025d.